International Journal of Heat and Mass Transfer 91 (2015) 711–724

Contents lists available at ScienceDirect

International Journal of Heat and Mass Transfer

journal homepage: www.elsevier.com/locate/ijhmt

General correlations among geometry, orientation and thermal performance of natural convective micro-finned heat sinks

Leonardo Micheli [a,*], K.S. Reddy [b], Tapas K. Mallick [a]

[a] Environment and Sustainability Institute, University of Exeter, Penryn Campus, Penryn, Cornwall TR10 9FE, UK
[b] Heat Transfer and Thermal Power Laboratory, Department of Mechanical Engineering, Indian Institute of Technology Madras, Chennai 600 036, India

ARTICLE INFO

Article history:
Received 18 December 2014
Received in revised form 5 August 2015
Accepted 5 August 2015
Available online 24 August 2015

Keywords:
Micro fins
Natural convection
Experimental
Passive cooling

ABSTRACT

The interest in micro-technologies has increased in the last decades, because of the low volumes and high performance granted by their application. Micro-fins can find application in several fields, such as power electronics, concentrating photovoltaics and LED. Although micro-technologies have been widely applied in cooling, there is still a lack of knowledge on the thermal behavior of micro-finned heat sinks under natural convective conditions. In the present study, the correspondences between fin geometries and heat transfer coefficients, as well as the effects of the orientation, are experimentally investigated using silicon micro-finned heat sinks with different geometries. The heat sinks are made of 5 cm × 5 cm squared silicon wafer and the fin height ranges between 0.6 mm and 0.8 mm, the spacing between 0.2 mm and 0.8 mm and the thickness between 0.2 and 0.8 mm. Power loads higher than those considered in previous works are studied. The experimental setup is validated using a software simulation and the Nusselt number correlation available in literature. The influence of the fin thickness on this parameter is analyzed and a modified correlation is proposed. Also, the effect of the radiative heat exchange on the overall heat transfer is considered and commented. An analysis of the uncertainty is conducted and reported too.

1. Introduction

Cooling, intended as removal of waste heat, is one of the major issues in many electronic applications, industrial processes, and power generation systems. Cooling technologies are usually classified in active or passive. An active system requires mechanical or electrical power in input. A passive cooling system does not require any power in input, because it just exploits the natural laws: these technologies are usually much simpler and less expensive that the active ones.

Among the passive cooling systems, fins represent one of the most common solutions. The enhancement in heat transfer is essentially achieved by increasing of exchanging surface. Macro-fin arrays have been widely investigated and are a proved and well-known solution, extensively used in many circumstances. Nagarani and his team [1] grouped the researches on fins into two categories: (a) the determination of the profile of the fin for a given quantity of heat transfer rate, and (b) the determination of the fin dimensions for a given fin form and a desired cooling rate. Bar-Cohen and his colleagues [2,3] presented a methodology to optimize the design of finned heat sink in natural convection. Dayan et al. [4] first investigated the behavior of downward facing macro-finned heat sinks in natural convection. In 2012, Do et al. [5] reported the results of their research on a tilted natural convective, plate-finned heat sink, showing the effects of the inclinational angle on the thermal exchange at macro scale. Recently, Tari and Mehrtash [6,7] have further investigated the performance of tilted finned heat sink.

In a world that is moving in the direction of micro-scaled electronic products, the interest around micro-cooling technologies, such as micro-fins, is quickly increasing: they assure faster performance, requiring both less space and less material than the macro-scale coolers. Micro cooling technologies have been already extensively researched, for electronic cooling purposes mainly [8]. This interest has rapidly grown in the last two decades [9] and has been driven by the necessity of more-efficient coolers to manage the heat waste produced by miniaturized electronic components [8]. Passive micro-finned heat sinks can be applied in many circumstances, such as electronics [10], solar power generation [11] and LED applications [12]. These technologies generate high rate of waste heat that needs to be quickly, cost-effectively and high-efficiently removed, but further investigations are still required. So far, active cooling technologies have been mainly employed [13], but the use of micro-fins in a natural convective cooling has

* Corresponding author. Tel.: +44 (0) 1326259478.
E-mail addresses: l.micheli@exeter.ac.uk (L. Micheli), ksreddy@iitm.ac.in (K.S. Reddy), t.k.mallick@exeter.ac.uk (T.K. Mallick).

http://dx.doi.org/10.1016/j.ijheatmasstransfer.2015.08.015
0017-9310/

Nomenclature

A	surface
F	view factor
g	gravitational acceleration
H	fin height
h	heat transfer coefficient
h_{tot}	average heat transfer coefficient
I_{DC}	current supplied in input
k_{air}	thermal conductivity of air
L	length of the array
N_{fins}	number of fins
Q	heat power
Q_{in}	power in input
Q_r	radiative heat through the fins
r	hydraulic radius
s	fin spacing
t	fin thickness
T_{amb}	ambient temperature
t_b	base thickness
T_{back}	temperature of the back surface of the case
v	kinematic viscosity of the air
V_{DC}	voltage supplied in input
W	width of the array
x	geometric parameter
x_μ	micro-fin global shape parameter
y	geometric parameter

Dimensionless numbers

Nu	Nusselt number
Pr	Prandtl number
Ra	Rayleigh number (based on characteristic length)
Ra_r	Rayleigh number (based on hydraulic radius)

Greek symbols

α	Thermal diffusivity of air
β	Volumetric thermal expansion
ε	Emissivity
σ	Stephan-Boltzmann constant

Subscripts

fins	Refers to the finned array
flat	Refers to the flat sample
i	Refers to the *i*-wall of the fin
loss	Refers to the losses happening on the case
tot	Refers to the combined radiative and convective exchange

Prefixes

U	Uncertainty

the potential to grant benefits both in terms of heat dissipation and cost saving [14].

Micro-fins can address the requirements for smaller volumes and lower costs that are currently sought after by industries and customers. In the light of developing a method to optimize the design of natural convective micro-heat sinks, the scientific community needs to widen the knowledge of the basics of convective heat transfer at micro-scale. The behavior of the heat transfer coefficient, as well as different heat sink metrics, has to be investigated. There is a number of works focusing on micro-fins, but only few of them investigated their application in a passive, natural convective environment. Shokouhmand and Ahmadpour [15] presented a numerical investigation about heat transfer from a top facing micro-fin array heat sink. They demonstrated that radiation can contribute up to 22% of the total heat transfer: the radiative exchange need to be considered when the heat behavior of micro-scaled heat sinks is analyzed. Kim et al. [16] demonstrated the impossibility of using the macro-fin heat transfer correlations for micro-scaled systems. The authors presented a first important investigation on natural convective micro-fin arrays, proving that the 100 to 200 μm-high fins used in their study could produce an enhancement in the thermal exchange up to 10%. They showed that the orientation effect can be neglected for vertical and horizontal micro-fin arrays and demonstrated that the convective heat transfer increases with increasing the spacing and the temperature difference between heat sink and ambient. Mahmoud et al. [17] investigated the thermal effect of 0.25 to 1.00 mm-high fins on copper heat sinks. In their work, the authors considered an upward facing array, uniformly heated by an electrical mat, with input powers ranging from 0.2 to 1.6 W. Their results showed that the values of convective heat transfer coefficient increased while increasing the fin spacing or decreasing the fin height. In their work, the authors did not take into account the effect of fins thickness on the thermal exchange.

In the present study, different 5 cm-wide squared heat sinks are studied under different power inputs, with the aim of extending the studies of the previous researchers. Firstly, the effects of the fin geometry are investigated for power loads higher than previously considered, in order to give a contribution towards the optimization of geometries for micro-finned heat sinks. In particular, the correlation between thickness and heat transfer is analyzed for the first time and commented. Based on that, a new correlation for determining the Nusselt number in micro-fins application is proposed. Secondly, an experimental comparison between the performance of plate fins and pin fins is reported. The previous micro-fins researches used to consider the same conditions, horizontal upward facing or vertical micro-finned heat sinks. In real applications, instead, the designer might be forced to orientate the heat sinks in different, less-effective directions, such as in downward facing position [4]. For this reason, the third scope of this paper is to report the differences in thermal performance between an upward facing and a downward facing micro-fins array.

2. Experimental apparatus

Each micro-finned heat sink exploited in this study has been produced by a 1.4 mm thick squared wafer, made of undoped silicon and sized 5 cm × 5 cm. Nine different fin geometries are tested and compared with a flat silicon wafer. Two fin types are considered: parallel rectangular plate fins (Fig. 1a) and square pin fins (Fig. 1b). The fins dimensions have then been measured using a microscope and are reported in Table 1, according with the nomenclature shown in Fig. 1. The micro-finned arrays have been firstly designed using a CAD software package and then fabricated through a dicing machine.

A schematic of the experimental setup is shown in Fig. 2 and has been developed similarly to those already referenced in literature [16,17]. The arrays are heated using 10 W flexible heaters (Omega KHLV-202/2.5), bonded through a conductive adhesive (3 M tape 966, 0.18 W/mK). The samples are held in an 8 cm × 8 cm case, made of a 1 cm-thick fiber thermal material

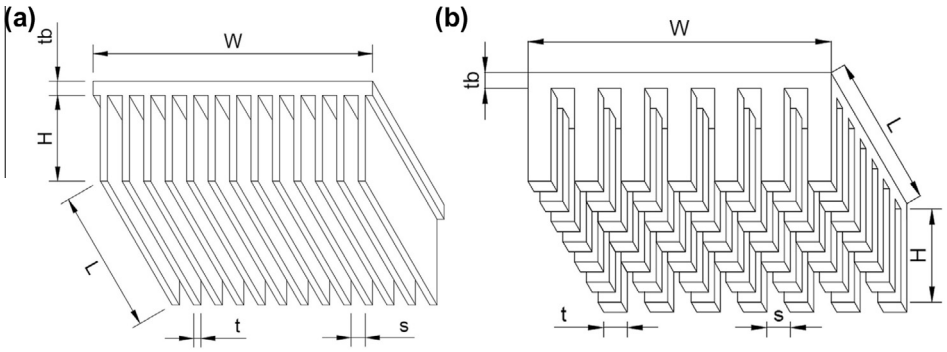

Fig. 1. Description of the parameters: (a) plate fin array, and (b) pin fin array.

Table 1
Fin dimensions.

Type	Width W (mm)	Length L (mm)	Fin thickness t (μm)	Fin spacing s (μm)	Fin height H (μm)	Base thickness t_b (μm)	Number of fins, N_{fin}
Flat	49.9	49.9	–	–	–	–	–
Plate fin	50.0	49.7	200	200	600	800	121
Plate fin	49.8	49.8	200	200	800	600	124
Plate fin	50.0	49.9	200	800	600	800	50
Plate fin	50.0	49.9	400	800	600	800	41
Plate fin	50.1	49.9	800	400	800	600	42
Plate fin	49.8	49.9	800	800	600	800	31
Pin fin	49.8	49.8	200	200	600	800	15376
Pin fin	50.2	50.0	400	400	600	800	3844
Uncertainty	0.05%	0.05%	4%	4%	6%	6%	–

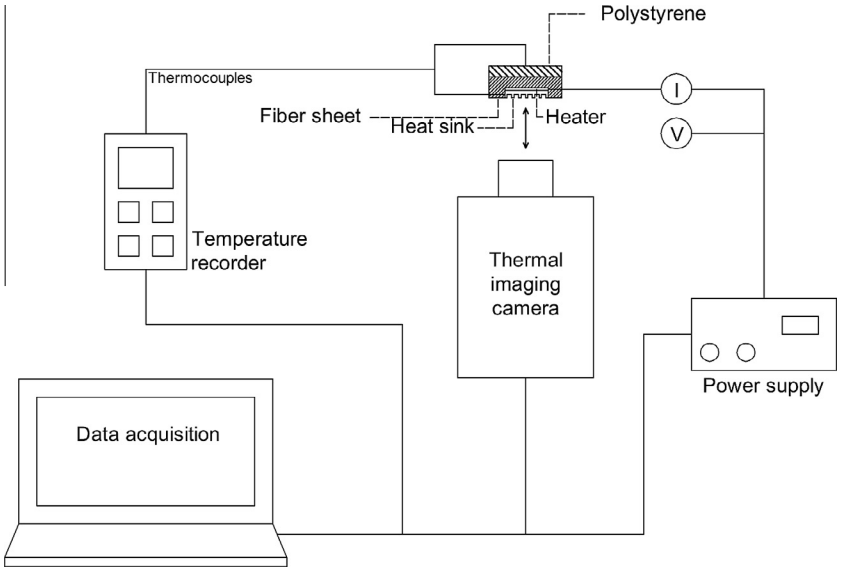

Fig. 2. Schematic of the experimental setup.

(0.05 W/mK). An additional 1 cm-thick polystyrene block (0.03 W/mK) is used to minimize the heat losses from the back surface. The sample is slot into the case and held through the contact between the case's pocket walls and the sample's sides. The sides of the sample which are perpendicular to the fins (W, in Fig. 1a) face the ambient, in order not to obstacle the air to flow through them.

The power input of the heater is controlled through a DC power supply (Weir 413D), ranged between 0 and 10 W using the analogical voltage control. Both current and voltage are measured using two digital multimeters (Fluke 115 and Fluke 8050A respectively). The maximum temperature of the silicon arrays is measured through a thermal imaging camera (FLIR T425). The emissivity of the silicon wafer, required in input by the thermal imaging camera, is set to 0.72 and is considered constant for the range of temperatures experienced in this work (25–200 °C) [16,18]. It is calculated by measuring the reflectance in a Perkimeter Lambda 1050 spectrometer and then applying the Kirchhoff's law. The emissivity used for the infrared imaging is obtained as the average of the emissivity across the wavelength range the thermal imaging camera works (750–1300 μm). The thermal imaging camera is placed

30 cm away from the sample. Two K type thermocouples are placed on the sides of the fins. The contact between thermocouples and sample's walls is ensured using a high temperature Kapton adhesive tape (Tesa 51408). Three more K type thermocouples are used to measure the temperature of the air in proximity of the samples and a last one is placed at the center of the back surface of the insulating material. A 12-Channel Temperature Recorder (Omega RDXL12SD) is used to record the thermocouples measurements. The room temperature is kept constant at 25 °C and checked through a digital thermohygrometer (Testo 608-H1).

In order to isolate the fins array from the external interferences, the sample is placed inside a 25 cm × 25 cm × 25 cm box open on top [16] and made of fiber thermal insulating sheet. On a side of the box, a 10 cm × 10 cm removable opening is placed: while under test, it is keep closed, and it is open only to let the thermal imaging camera to focus on the fins array at steady state. The setup reaches the steady state conditions in less than 20 min from the moment the current starts flowing across the heater at ambient temperature. Once at steady state conditions, the temperatures are recorded in 10 s: each test is conducted three times and the average value of the outputs is considered. Fig. 3 shows the behaviors of three thermocouples when the flat wafer is tested downward with an input power of 7.5 W: thermocouple (a) measures the transient thermal behavior of the sample, thermocouple (b) the insulating case's temperature and thermocouple (c) the ambient temperature (c). The thermocouples data are recorded each two seconds and are stored in a database.

3. Data analysis and validation

3.1. Thermal losses

The aim of this paper is to investigate, in different conditions, the heat transfer coefficients of micro-fins arrays (h_{fins}), defined as:

$$h_{fins} = \frac{Q_{fins}}{A_{fins} \cdot (T_{fins} - T_{amb})} \tag{1}$$

where Q_{fins} is the heat dissipated through the fins by convection, A_{fins} is the area of the finned surface, T_{fins} corresponds to the fins temperature, measured by the thermal imaging camera and considered uniform across the fin array, and T_{amb} is the ambient temperature, registered by the thermocouples. The heat transfer coefficients of the flat plate (h_{flat}) can be calculated similarly, taking into account the flat sample surface (A_{flat}) and its temperature (T_{flat}). The heat transfer coefficients are strongly dependent on the area of the surface: compared to the flat plane, the addition of fin is expected to increase both the exchanging surface and the exchanged heat. The power load (Q_{fins}) need to be considered after the radiated heat transfer (Q_r) and the losses that happen on the back and the sides of the samples (Q_{loss}), in order to estimate the fins' heat transfer coefficient in the most accurate way. It is thereby expressed as:

$$Q_{fins} = Q_{in} - Q_r - Q_{loss} \tag{2}$$

where Q_{in} represents the heat produced by the heating film, calculated by multiplying the voltage (V_{DC}) and the current (I_{DC}) provided by the power supply:

$$Q_{in} = V_{DC} \cdot I_{DC} \tag{3}$$

The heat dissipated by the flat plate (Q_{flat}) is calculated similarly to Q_{fins}. The total heat transferred by radiation from the fins array (Q_r) is expressed by the Stefan–Boltzmann equation as sum of the radiative heat transfers happening in the different fin surfaces (top, side, face and base):

$$Q_r = \sum_i \varepsilon \cdot \sigma \cdot A_i \cdot F_{i,k} \cdot (T_{fins}^4 - T_{amb}^4) \tag{4}$$

where ε is the emissivity of silicon, σ is the Stefan–Boltzmann constant ($5.67 \times 10^{-8} Wm^{-2}K^{-4}$), A_i is the area of the correspondent i-surface of the fins, $F_{i,k}$ are the view factors between the surfaces i and k. The emissivity of silicon is set to 0.78. The view factors depend on the geometry of the fins and are different for the various surfaces. They have been calculated with the model presented by [19]. The wall of a fin (Fig. 4a) exchanges radiative heat with the base (Fig. 4b), the wall of the adjacent fin (Fig. 4c) and the ambient (Fig. 4d).

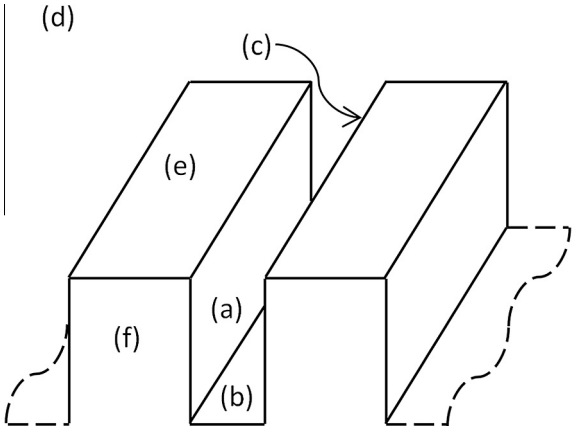

Fig. 4. Schematic of the micro-fin array: the fin walls (a), (c), (e), (f); the base (b); and the ambient (d).

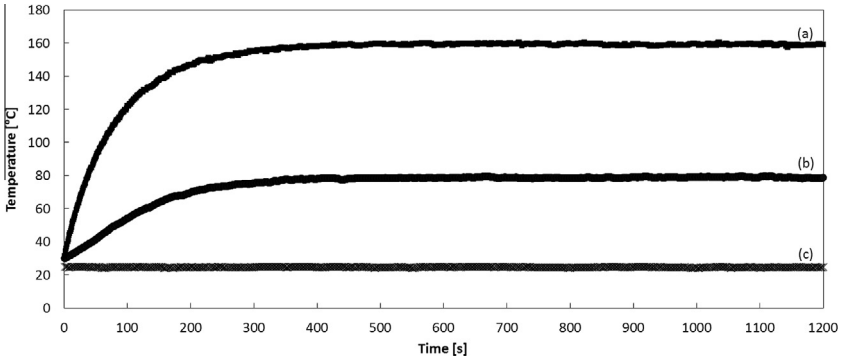

Fig. 3. The transient temperatures of the flat silicon wafer facing downwards, with a power input of 7.5 W: (a) temperature of the sample's surface, (b) temperature of the back surface of the insulating material and (c) ambient temperature.

The view factor between the fin wall and the base ($F_{a,b}$) can be estimated as [19]:

$$F_{a,b} = \frac{1}{\pi \cdot y} \cdot \left\{ \begin{array}{l} y \cdot \tan^{-1}\left(\frac{1}{y}\right) + x \cdot \tan^{-1}\left(\frac{1}{x}\right) - \left(x^2+y^2\right)^{0.5} \cdot \tan^{-1}\left(\frac{1}{\left(x^2+y^2\right)^{0.5}}\right) + \\ + \frac{1}{4} \cdot \ln\left(\frac{(1+x^2)\cdot(1+y^2)}{1+x^2+y^2} \cdot \left(\frac{y^2\cdot(1+x^2+y^2)}{(x^2+y^2)\cdot(1+y^2)}\right)^{y^2} \cdot \left(\frac{x^2\cdot(1+x^2+y^2)}{(x^2+y^2)\cdot(1+x^2)}\right)^{x^2}\right) \end{array} \right\} \quad (5)$$

where $x = s/L$ and $y = H/L$.

The view factor between two adjacent fins' walls ($F_{a,c}$) is estimated as [19]:

$$F_{a,c} = \frac{2}{\pi \cdot x \cdot y} \cdot \left\{ \begin{array}{l} \ln\left(\frac{(1+x^2)\cdot(1+y^2)}{1+x^2+y^2}\right)^{0.5} + x \cdot \left(1+y^2\right)^{0.5} \cdot \tan^{-1}\left(\frac{x}{\left(1+y^2\right)^{0.5}}\right) + \\ + y \cdot \left(1+x^2\right)^{0.5} \cdot \tan^{-1}\left(\frac{y}{\left(1+x^2\right)^{0.5}}\right) - x \cdot \tan^{-1} x - y \cdot \tan^{-1} y \end{array} \right\} \quad (6)$$

where $x = H/s$ and $y = L/s$.

The view factor between the fin wall and the ambient ($F_{a,d}$) is then estimated using the equation for an enclosure with four surfaces [10]:

$$F_{a,b} + F_{a,c} + F_{a,d} = 1 \quad (7)$$

The view factor between the fin's base and the fin's wall ($F_{a,b}$) is obtained exploiting the reciprocity relation [10]:

$$A_a \cdot F_{a,b} = A_b \cdot F_{b,a} \quad (8)$$

The view factors of the surfaces "e" and "f" are equal to 1. According to this model, the contribution of the radiative exchange increases with the power input. Out of a gross 10 W power input supplied to the heater, a percentage ranging between 35 and 42% is dissipated because of radiative exchange of the fins.

The Q_{loss} are due to the heat dissipation happening on the unfinned surfaces of the assembly: these are the radiative and the convective thermal exchanges on the sides and on the back of the structure. The radiative component has been estimated considering the emissivity of polystyrene (0.60) and fiber sheet (0.85) and a view factor of 1. The convective exchange happening on the back surface of the insulator has been calculated considering the equations reported in [20]:

$$h_{loss} = \frac{k_{air}}{L} \cdot Nu_{loss} \quad (9)$$

where k_{air} is the thermal conductivity of the air and Nu_{loss}, the Nusselt number, which can be calculated accordingly to the orientation of the surface [20]:

$$Nu_{loss} = 0.13 \cdot (Ra)^{1/3} \quad \text{if the surface is horizontal and faces upwards;} \quad (10)$$

$$Nu_{loss} = 0.59 \cdot (Ra)^{1/4} \quad \text{if the surface is vertical;}$$

$$Nu_{loss} = 0.58 \cdot (Ra)^{1/5} \quad \text{if the surface is horizontal and faces downwards.} \quad (12)$$

Ra is the Rayleigh number, which is defined as:

$$Ra = \frac{g \cdot \beta \cdot \mathrm{Pr} \cdot s^4 \cdot (T_{back} - T_{amb})}{L \cdot v^2} \quad (13)$$

where g is the gravitational acceleration, β is the volumetric thermal expansion of the air, Pr is the number of Prandtl, v is kinematic viscosity of the air and T_{back} is the temperature measure by the thermocouple placed on the back surface of the insulator. All the properties have been evaluated considering an air temperature of $(T_{back} + T_{amb})/2$, with the exception of the thermal expansion, evaluated at ambient temperature [19].

All the tests are conducted for $Ra > 10^6$, condition needed for applying the equations of convective heat transfer for inclined surface. The losses averagely accounted for 26% of the total power input, with comparable contributions from the convective and the radiative heat transfers.

3.2. Measurements uncertainty

The main output of the present research is h_{fins}, which is obtained by computing experimental data that are subject to uncertainty. The overall uncertainty is calculated accordingly to the propagation of error for independent variables [21]:

$$\frac{Uh_{fins}}{h_{fins}} = \sqrt{\left(\frac{UQ_{fins}}{Q_{fins}}\right)^2 + \left(\frac{UA_{fins}}{A_{fins}}\right)^2 + \left(\frac{UT_{fins}}{T_{fins} - T_{amb}}\right)^2 + \left(\frac{UT_{amb}}{T_{fins} - T_{amb}}\right)^2} \quad (14)$$

where the uncertainties are indicated with the prefix "U". The array surface can be calculated with an uncertainty of ±4%. T_{fins} is measured with the thermal imaging camera, which has an uncertainty of measurement of ±0.2%. The uncertainty on the emissivity cannot be neglected [16] and is considered equal to ±0.2. This value corresponds to an additional fins temperature discrepancy of ±3.5 °C. T_{amb} is obtained as average of the thermocouples measurements, read from the temperature recorder (accuracy:±0.4%). The thermocouple data are adjusted according to the offset measured in a preliminary investigation: an uncertainty of ±1.0 °C is considered. The maximum uncertainty is found to be ±8.25%, and occurred at low power inputs. This value falls within the range reported in similar studies [16,17] and is represented by the error bars in all the figures reported in the paper. Where different metrics are used, the error bars are calculated following the same methodology.

3.3. Numerical validation of the experimental setup

In order to verify the reliability of the experimental setup, a computation analysis is carried out using the "Heat Transfer" module of COMSOL Multiphysics 4.4. The flat plate sample is modeled and the outputs of the simulation are compared with the experimental results. The heater is modeled as a 0.254 mm-thick copper plate, bonded to the 1.4 mm thick silicon sample (Fig. 5a.3) through the adhesive, represented as a thermal resistive layer (0.06 mm-thick, 0.18 W/mK). Both the heater and the silicon sample size 5 cm × 5 cm. The heater is set as a "Heat Source", which requires the total thermal power in input. The insulating structure is reproduced around samples: it is composed by a 1 cm-thick fiber sheet (0.05 W/mK, 1900 kg/m^3, 1369 J/kgK; Fig. 5a.2), back-covered with a 1 cm-thick polystyrene block (0.33 W/mK, 960 kg/m^3; Fig. 5a.1). The interface contact between the heater and the insulator is considered as a 0.5 mm air layer.

The "Convective Heat Flux" function is applied to all the external surfaces: the heat transfer coefficient is automatically defined by COMSOL for each surface accordingly to its orientation and geometry. All the external surfaces are set to exchange heat with the environment. The emissivity is fixed: 0.78 for silicon, 0.85 for the fiber sheet and 0.60 for the polystyrene. The automatic "phy sics-controlled" mesh generator is chosen and a "finer" size is selected. The simulator solved 242803 degrees of freedom (Fig. 5), converging to a solution in 50 s.

The maximum temperature of sample's external surface predicted by COMSOL is then compared with that measured by the thermal imaging camera. A comparison between the two images is reported in Fig. 6. Four different thermal inputs are considered: 2.5 W, 5 W, 7.5 W, and 10 W. All the tests are carried out in stationary mode.

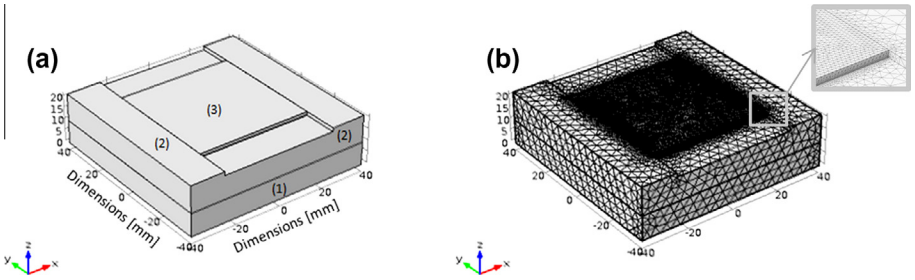

Fig. 5. The geometry of the experimental setup modeled in COMSOL (a): the polystyrene block (1), the fiber sheet case (2), and the flat plane sample (3). In (b), the tetrahedral mesh is reported.

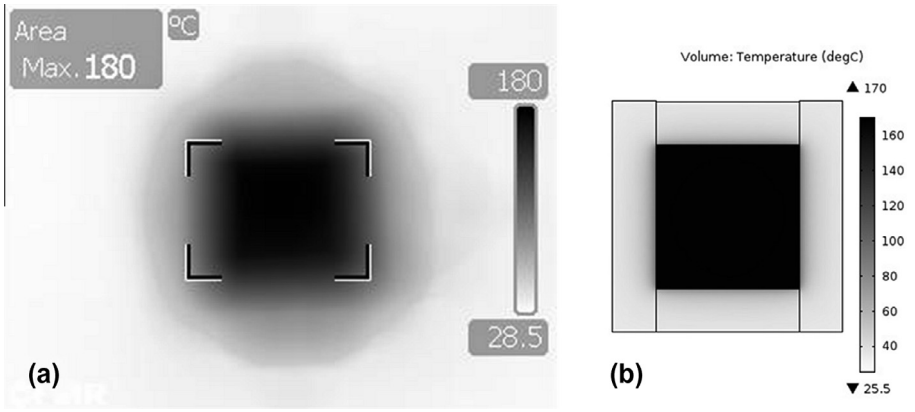

Fig. 6. Comparison between the top view of the sample taken from the thermal imaging camera (a) and the COMSOL model results (b). All the temperatures are shown in °C. Conditions: sample facing upwards, heat power input 10 W.

The difference between the experimental and the simulated data ranges between 2 °C (for the lowest power) and 10 °C (for the highest power). These results are in line with those reported by [17]: the discrepancies are due to a number of factors. In particular, the model takes into account fixed values of the materials' properties (e.g. thermal conductivity, and density), whereas these properties, in the real case scenario, strongly depend on the temperature. Moreover, some divergences between the thermal contact resistance modeled by COMSOL and those recorded in the experimental setup might have contributed to this discrepancy.

In order to understand the reliability of the experimental setup, the heat transfer coefficients obtained experimentally and numerically are compared. The heat transfer coefficients are determined as for (1), by removing the heat transferred by radiation and the thermal losses. As shown in Fig. 7, the heat transfer coefficients are found to increase with the power input. As expected, the increasing rate lowers at high power input: this is due to the contribution of the radiative heat transfer, which, at constant ambient temperature, increases with the forth power of the surface temperature. The numerical model consistently overestimates the heat transfer coefficients in upward facing conditions, with an average discrepancy of 6.07% and a maximum of 7.18%. In the downward facing conditions, instead, the average difference drops to 2.84%, with a maximum of 4.66%. All these discrepancies fall within the

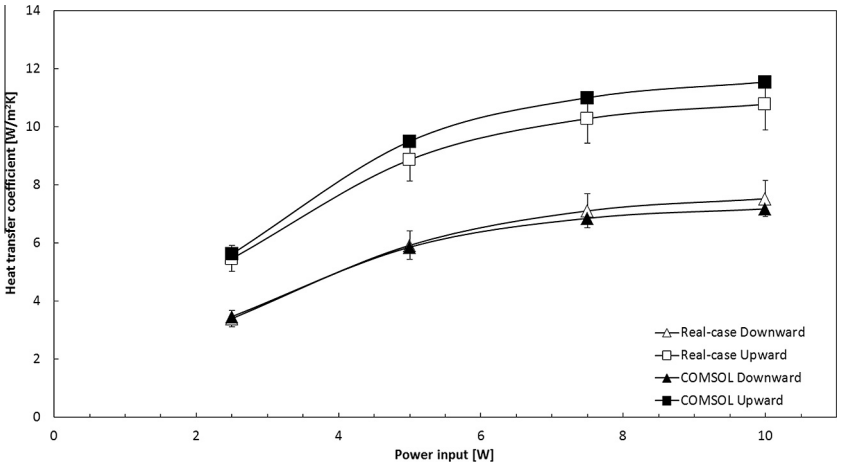

Fig. 7. Comparison between the COMSOL simulation outputs and the experimental real-case measurements.

uncertainty expected for this experimental setup and can be considered acceptable for an experimental investigation on natural convection [22].

A 2D model is then developed using the same geometry to study the dynamic behavior of the air in the experimental setup. The flat wafer (Fig. 8a), the fiber sheet (Fig. 8b) and the polystyrene (Fig. 8c) are reproduced using the experimental dimensions specified before and placed inside a 25 cm × 25 cm square (Fig. 8d), filled with air. The square has adiabatic walls, with an open boundary condition at the top to let the air to flow. A power input of 10 W is considered and an initial temperature of 25 °C is set for all the components. The results of the simulation are shown in Fig. 8: the hot air moves upward at the center of the setup, whereas the cold flow moves downward from the edges of the box.

4. Results and discussion

4.1. Effects of fin thickness, spacing and height

The correlations between fins geometry and thermal performance are investigated in order to improve the temperature range considered in [17], which is limited to power loads up to 1.6 W and maximum temperatures in the order of 100 °C. Mahmoud and his colleagues proved that the values of convective heat transfer coefficient increases when increasing the fin spacing and decreasing the fins height. The experimental data collected in this study confirm these behaviors: the heat transfer coefficient is found to be enhanced by increasing the fin spacing (Fig. 9) or decreasing the fin height (Fig. 10).

The effects of the fin thickness on the heat transfer coefficient are investigated as well. As shown in Fig. 11, the heat transfer coefficient increases when the fin thickness increases. In micro-scale, within the narrow space between two adjacent fins, the conduction is dominant over the natural convection [16], and, thus, the volume of air within two micro-fins transfers heat mainly by conduction. Therefore, increasing the fin thicknesses while keeping the spacing constant increases the high-conductive volume of silicon compared to the low-conductive volume of air, so the overall thermal conductance is enhanced. For this reason, the thickness of micro-fin is a dimension to be taken into account when dimensioning an optimal micro-finned heat sink.

As noted by [17], the heat transfer coefficient tends to increase when the temperature increases. Although, at the higher temperature differences experienced in the present study, the enhancement of the heat transfer coefficient is lower and, in each test, the coefficient reaches a maximum value, before starting decreasing. This is probably due to the increased contribution of radiative heat transfer, which is proportional to the fourth power of the temperature of the radiative walls and, so, grows at rate higher than convection when the temperature difference rises.

4.2. Nusselt number correlation

Natural convection conditions are usually described by dimensionless numbers, in order to reduce the number of total variables. The Nusselt number compares the heat transfer enhancement in natural convection and that in conduction across a fluid layer [22] and can be used to estimate the heat transfer coefficient. For upwards micro-fins array, the following empirical equation has been proposed by Kim et al. [16]:

$$Nu = 1.18 \cdot \left[Ra_r \cdot \left(\frac{r}{H}\right)^4 \cdot \left(\frac{r}{L}\right)^4 \right]^{0.147} \tag{15}$$

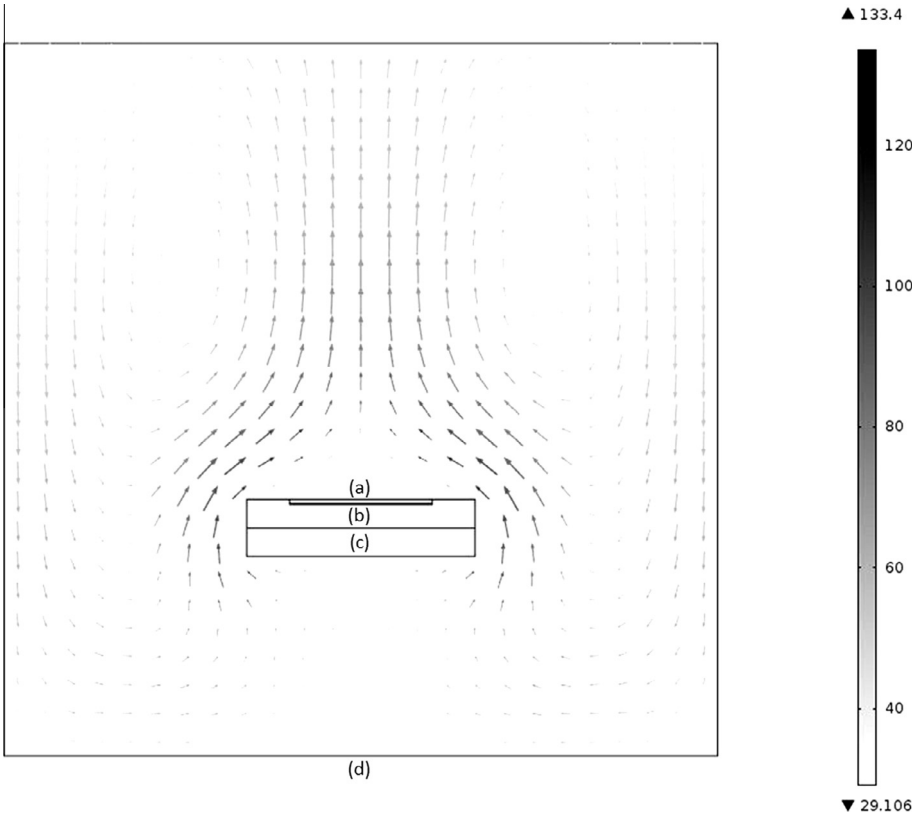

Fig. 8. Velocity field of the air inside the experimental setup: the flat silicon wafer (a), the 1 cm-thick fiber sheet (b), the 1 cm-thick polystyrene block (c) inside the 25 cm × 25 cm box (d), open on top. The thin heater is reproduced and is placed between (a) and (b). The length of the arrows represents the velocity (the longer, the faster), whereas the color represents the temperature (the darker, the hotter). The temperature scale, in °C, is shown on the right.

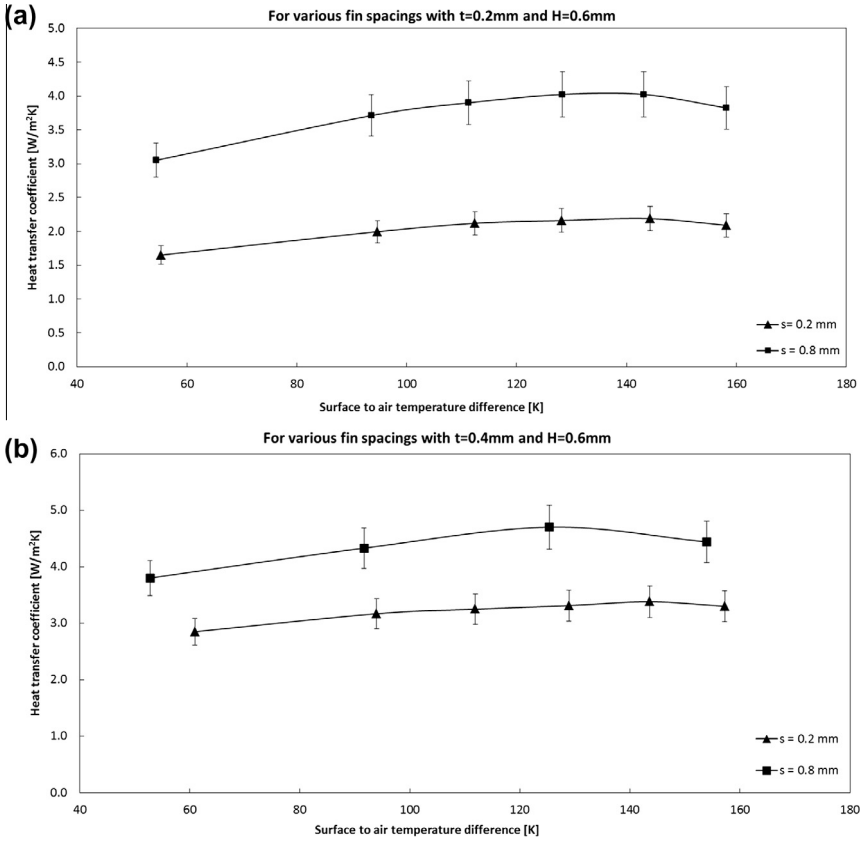

Fig. 9. Effects of fin spacing on the heat transfer coefficient. Fin spacing is varied with constant fin thickness and fin height: in (a) t = 0.2 mm and H = 0.6 mm; in (b) t = 0.4 mm and H = 0.6 mm.

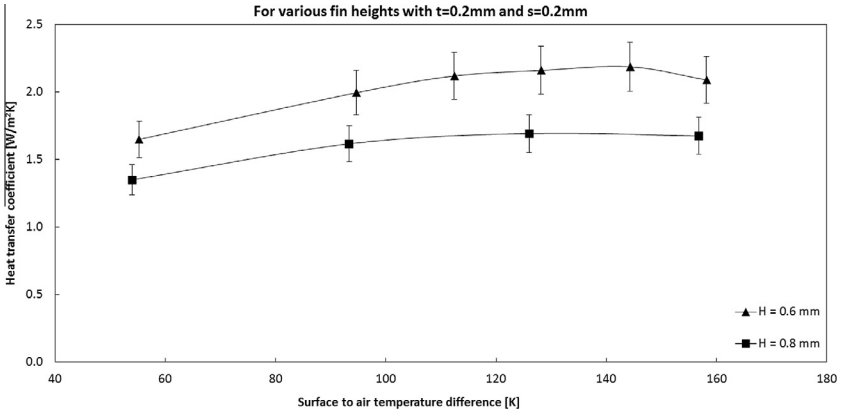

Fig. 10. Effects of the fin height on the heat transfer coefficient. Fin height is varied with constant fin thickness and fin spacing: t = 0.2 mm and s = 0.2 mm.

where r is the hydraulic radius and the Rayleigh number for micro-finned surfaces, derived from Eq. (13), is expressed as:

$$Ra_r = \frac{g \cdot \beta \cdot (T_{fins} - T_{amb}) \cdot r^3}{\nu \cdot \alpha} \tag{16}$$

where α is the thermal diffusivity of air (m^2/s), as reported by [23]. The hydraulic radius (r) for horizontal finned surfaces is expressed as [24]:

$$r = \frac{2 \cdot H \cdot s}{2 \cdot H + s} \tag{17}$$

The experimental Nusselt numbers, obtained by the present investigation, and the predicted Nusselt numbers show an average deviation of 10.59%. This value can be considered acceptable, taking into account the uncertainty reported by the authors of the correlation (6.3%) and that predicted in the present experimental investigation (8.25%). For this reason, the correlation can be considered verified for upward facing silicon micro-finned array, up to a maximum fin length of 50 mm.

As already pointed out in the paper, at micro-scale the fin thickness has an effect on the heat transfer coefficient, which is not accounted in (15). In the previous investigations a fixed thickness was considered: according to the present results, the average discrepancy gets wider when the thickness is increased (3% for t = 0.2 mm, 13% for t = 0.4%, 22% for t = 0.8 mm). As first approach, Eq. (15) is adapted as follow:

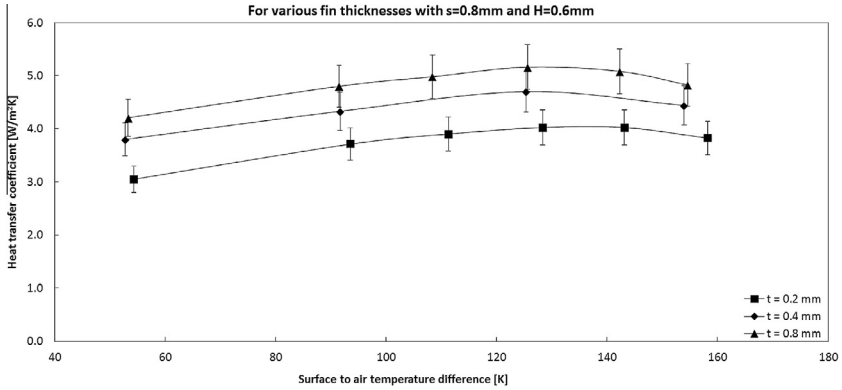

Fig. 11. Effects of the fin thickness on the heat transfer coefficient and the thermal resistance. Fin thickness is varied with constant fin spacing and fin height: s = 0.8 mm and H = 0.6 mm.

$$Nu^* = 1.18 \cdot \left[Ra_r \cdot \left(\frac{r}{H}\right)^4 \cdot \left(\frac{r}{L}\right)^4\right]^{0.147} \cdot \left[1 + \left(\frac{t}{r}\right)^2\right]^{0.147}$$
$$= 1.18 \cdot \left[Ra_r \cdot \left(\frac{r}{H}\right)^4 \cdot \left(\frac{r}{L}\right)^4 \cdot \left(1 + \left(\frac{t}{r}\right)^2\right)\right]^{0.147} \quad (18)$$

In Eq. (18), the Nusselt number increases when thickness is increased. Moreover, Nu^* equalizes Nu when $t \ll r$. This way, the average discrepancy is reduced to 6.05% and ranges between 5% and 8% at different thicknesses. Eq. (18) can be simplified by taking into account a new dimensionless parameter (called *micro-fin global shape parameter*, x_μ) that groups the micro-fin geometric dimensions at micro-scale:

$$x_\mu = \left(\frac{r}{H}\right)^4 \cdot \left(\frac{r}{L}\right)^4 \cdot \left(1 + \left(\frac{t}{r}\right)^2\right) \quad (19)$$

Eq. (18) therefore becomes:

$$Nu^* = 1.18 \cdot \left(Ra_r \cdot x_\mu\right)^{0.147} \quad (20)$$

In this way, it is possible to predict the coefficient of thermal performance of micro-fins by using the following equation:

$$h_{fins} = \frac{k_{air}}{L} \cdot Nu^* = 1.18 \cdot \frac{k_{air}}{L} \cdot \left(Ra_r \cdot x_\mu\right)^{0.147} \quad (21)$$

Despite the sample dimensions (H = 0.25–1.00 mm, L = 31.75 mm, S/H = 0.5–4) fell within the range of validity of Eq. (15), Mahmoud and his colleagues [17] reported a discrepancy of 29% among the experimental and the predicted Nusselt numbers. In the present study, the data of [17] have been analyzed using *Engauge Digitizer 4.1*. A maximum uncertainty of 1% has been found repeating the digitalization process twice. According to the acquired data, Eq. (15) consistently underestimates the Nusselt number of copper micro-fins with an average deviation of 26%, still too high to be considered due to the experimental and data-digitalization uncertainties only. Using the modified Nusselt number correlation in Eq. (18), instead, would reduce the discrepancies from 26% to 7.41%. The maximum and the minimum deviations obtained with the correlation in (18) are 20.59% and 0.62% respectively, and are both lower than those registered by using the correlation in (15) which are 35.99% and 16.59% respectively. This can be seen in Fig. 12 and in Fig. 13, where the predictions of (15) and (18) are compared with the data collected in the present study and the data reported by [17]. The data obtained by the correlation in (18), represented by the triangular markers (Δ), are consistently closer to the experimental data presented in this work (white squared markers, □) and to the referenced data reported by [17] (black squared markers, ■) than those obtained by the correlation in (15), represented by the crossed marker, ×.

A summary of the deviations achieved by the different correlations is shown in Table 2, both for the experimental data reported in the present paper and for the data of [17]. As clear in the table, the new correlation lowers the average, the maximum and the minimum deviation from both the considered dataset. As already stated, the most important reduction is registered for the data of

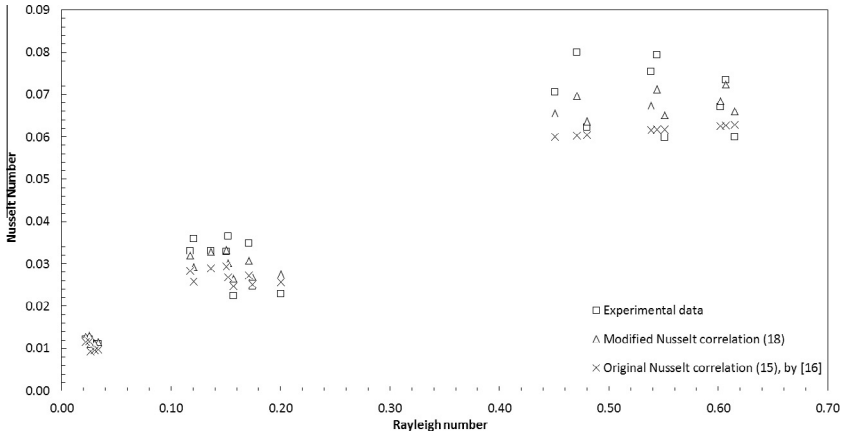

Fig. 12. Comparison of the experimental results (□), the original Nusselt correlation for micro-finned heat sinks (15) presented in [16] (×), and the modified Nusselt number correlation (Δ) presented in (18). Compared to the previous correlation the modified Nusselt number correlation reduces the average deviation of the experimental data from 10.59% to 6.05%.

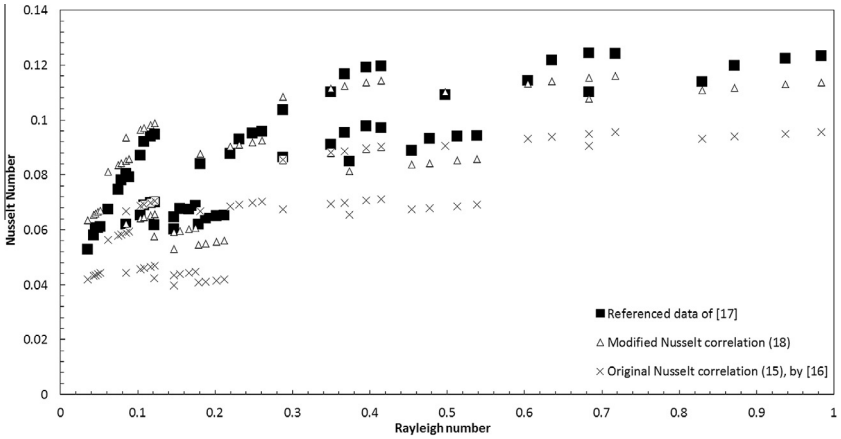

Fig. 13. Comparison of the Mahmoud referenced data (■) [17], the original Nusselt correlation for micro-finned heat sinks (15) presented in [16] (×), and the modified Nusselt number correlation (Δ) presented in (18). Taking into account the data reported by [17], the new correlation reduces the average deviation from 26% to 7.41%.

Table 2
Average, maximum and minimum deviation obtained by using the different Nusselt number correlations.

Data from	Range of *Ra*	Correlation	Average deviation (%)	Maximum deviation (%)	Minimum deviation (%)
Present paper	0.022–0.614	Original (15)	10.59	24.49	1.17
		Modified (18)	6.05	13.96	0.39
[17]	0.036–0.988	Original (15)	25.91	35.99	16.59
		Modified (18)	7.41	20.59	0.62

[17]: in that experimental setup, copper was the materials used for the heat sinks, instead of silicon, employed in [16]. When the volume between the adjacent fins is too small, air tends to behave like a solid material and present a high thermal resistance. So, the fin and the fin spacing would act as two parallel solid layers. The heat would then preferably flow through the high-conductive fin material and then be dissipated by convection from the fin top. Using a high conductive fin material, such as copper, more thermally conductive than silicon, would increase the heat flow through the fin. Moreover, a larger thickness would further decrease the thermal resistance of the fin: the thicknesses considered in [17] were higher than those considered by [16]. The combination of a higher conductive material and of thicker fins lead to the big deviation between the experimental data of [17] and those predicted by (15). For this reason, the contribution of the thickness cannot be neglected at microscale and has been accounted in (18). The modified correlation (18) can be considered available for H from 0.25 mm to 1.0 mm, L from 31.75 to 50 mm, and S/H from 0.2 to 2. For a more accurate Nusselt number estimation, further investigations are needed to understand the influence of thickness in a wider range of dimensions.

4.3. Plate fins vs pin fins

In this section, the performance of a plate fin and a pin fin arrays are compared. The two geometries are based on the same dimensions: s, t, H and t_b are the same. In order to have a result valid for a wide range of fins, two couples of pin/plate fins arrays are considered, whose dimensions have been shown in Table 1. Micro-fins are generally obtained through subtractive methods: the use of pin fins instead of plate fins reduces the volume of the heat sink and, in this case, the overall pin–finned wafer volume

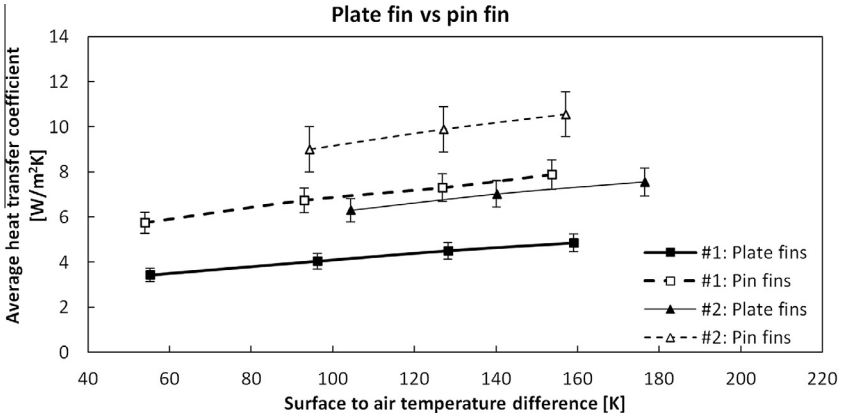

Fig. 14. Comparison between heat transfer coefficients in plate and pin fin configurations. The dimensions of fins are as follow: t = 0.2 mm, s = 0.2 mm, H = 0.6 mm (#1, ■ plate fins, □ pin fins) and t = 0.4 mm, s = 0.4 mm, H = 0.6 mm (#2, ▲ plate fins, Δ pin fins).

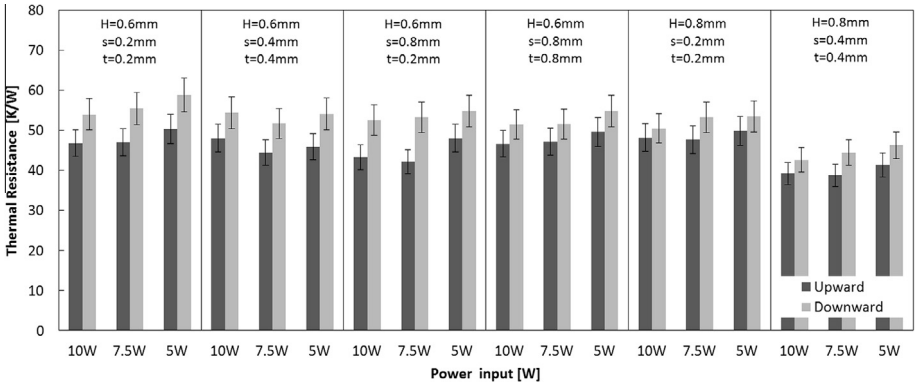

Fig. 15. Thermal resistance of the different plate fins: upward vs. downward.

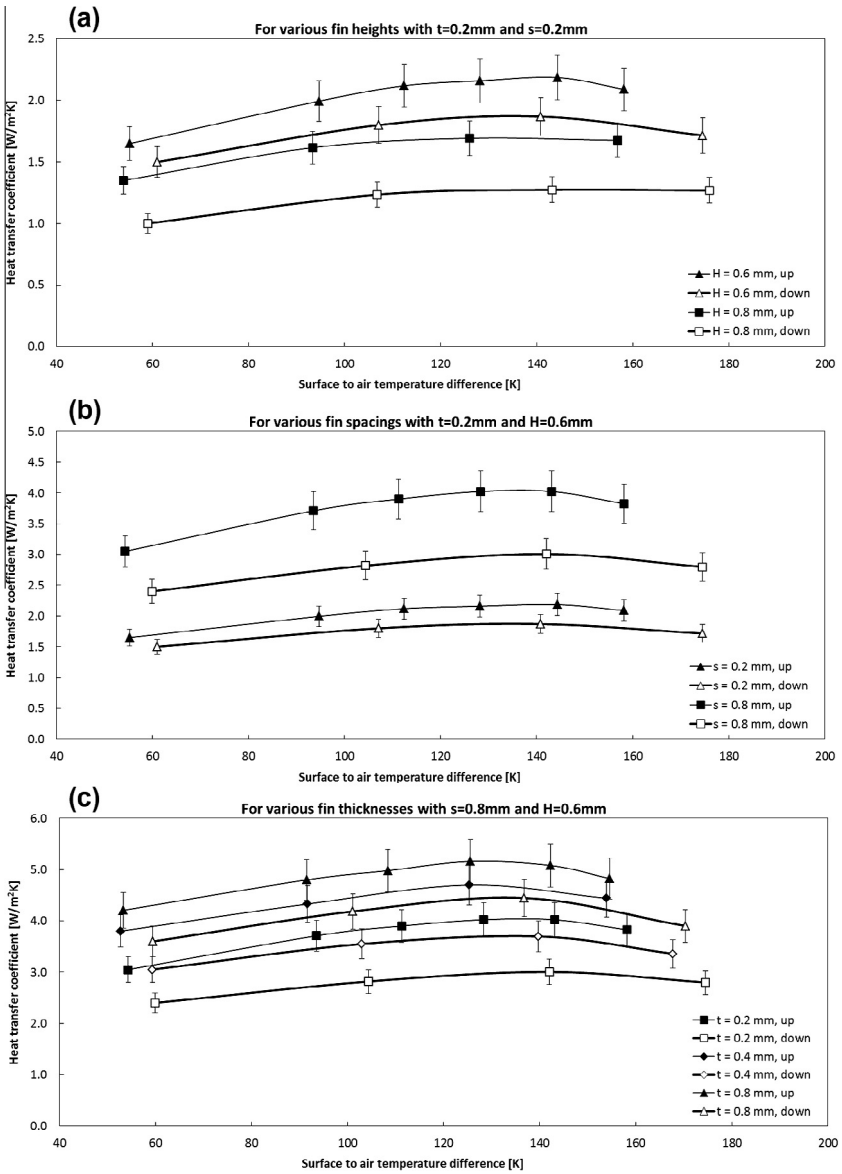

Fig. 16. Effect of geometry on the thermal behavior of downward facing plate-finned heat sink. In (a), fin height is varied with constant fin thickness and fin spacing (t = 0.2 mm and s = 0.2 mm). In (b), fin spacing is varied with constant fin thickness and fin height (t = 0.2 mm and H = 0.6 mm). In (c), fin thickness is varied with constant fin spacing and fin height (s = 0.8 mm and H = 0.6 mm).

is found to decrease by 13% compared to the plate-finned one. On the other hand, since in both the considered geometries the fin spacing is equal to the fin thickness, no change in surface is registered between the pin–finned and the plate-finned configurations. Despite that, the thermal exchange is expected to change: in a pin–finned geometry, an enhancement in extension of the fin base surface and a reduction of the top fin surface are registered. As already discussed, the convective thermal behaviors of these two geometries are different: the fin base exchange heat with the air trapped in the fin spacing, which in some configuration can behave similarly to an insulating layer, whereas the top surfaces of the fins are free to exchange heat with air in free convection. Moreover, changes in the radiative view factors are expected to further affect the heat transfer. In particular, the present study estimates the contribution of the radiative exchange using the model in [19] to determine the view factors. Since two different geometries are compared in this section, different models should have been used for estimating the view factors. In order not to have the comparison affected by the different models, it has been preferred to consider the overall heat exchanged by the fins, intended as sum of the radiative and convective heat transfers happening through the fins (Q_{tot}):

$$Q_{tot} = Q_{fins} + Q_r \tag{22}$$

A combined heat transfer coefficient, defined *average heat transfer coefficient* by [25], is then calculated:

$$h_{tot} = \frac{Q_{tot}}{A_{fins} \cdot (T_{fins} - T_{amb})} \tag{23}$$

As shown in Fig. 14, the pin fin has a better average heat transfer coefficient than the plate fin, so more heat is transferred from the heat sink by radiation and convection in pin fins than in plate fins. Because of the same surface, a higher heat transfer coefficient means that the pin finned configuration is able to transfer a larger amount of heat under the same temperature difference. So, the pin fins have the potential to increase the heat transfer and, at the same, to decrease the volume and the weight of the heat sink. A

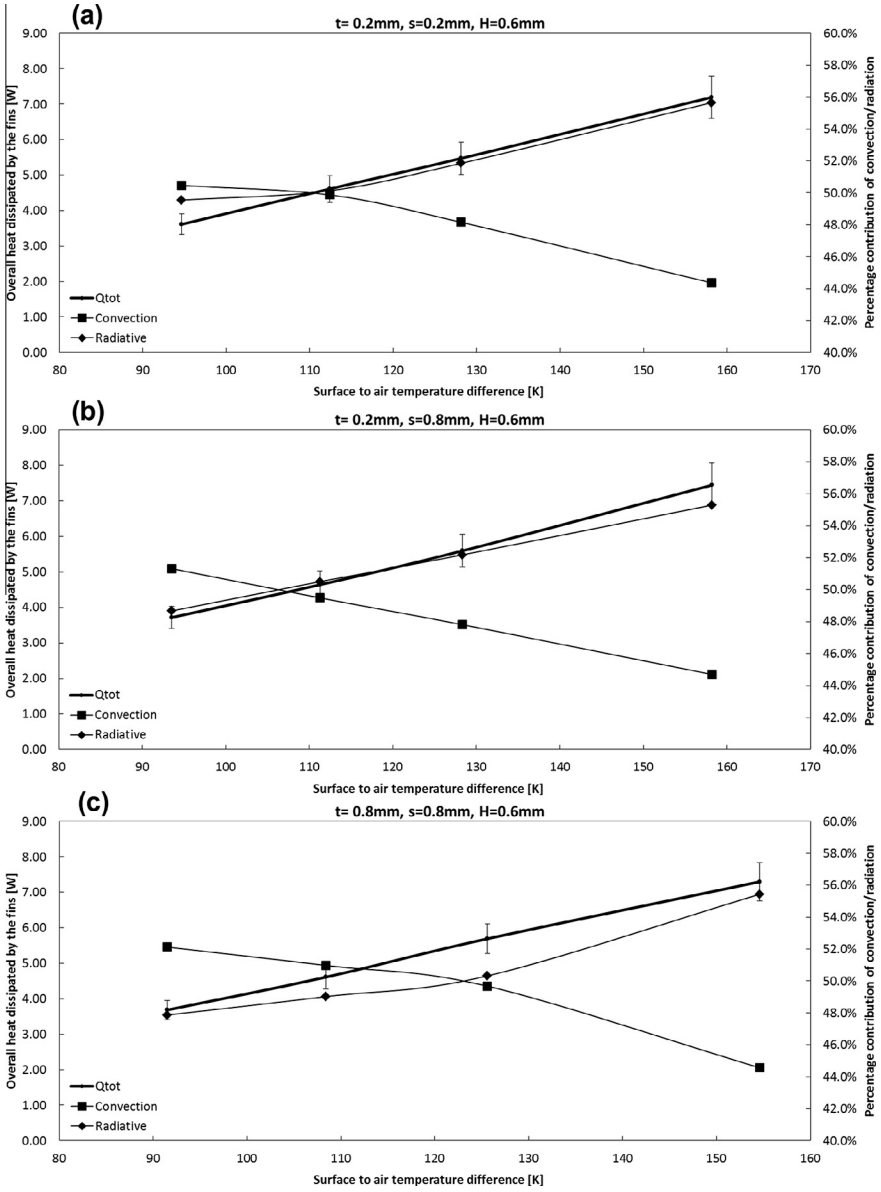

Fig. 17. Global heat exchange at different plate fin geometries. Three geometries are considered: t = 0.2 mm, s = 0.2 mm and H = 0.6 mm in (a); t = 0.2 mm, s = 0.8 mm and H = 0.6 mm in (b); t = 0.8 mm, s = 0.8 mm and H = 0.6 mm in (c).

more detailed analysis is required to explain in most appropriate way the physics behind this improvement in heat transfer, that is probably due to an higher radiative heat transfer rate, and to lead to the optimization of the geometry of micro-pin fin arrays.

4.4. Upwards vs downwards orientation

It is already known that a downward facing is not the best orientation for a heat sink under natural convection conditions [4]. This is confirmed also in the present experimental investigation, where the thermal resistance (R_{fins}) is considered:

$$R_{fins} = \frac{T_{fins} - T_{amb}}{Q_{fins}} \tag{24}$$

Fig. 15 collects the thermal resistances of different heat sinks under different power inputs: an average discrepancy of 12% in thermal resistance is recorded between the same heat sink in upward and downward facing conditions and the percentage differences are found to be constant under different power inputs.

As shown in Fig. 16, the behavior of the downward facing heat sink is similar to that of the upward facing: the heat transfer coefficients increases when increasing the fin thickness and the fin spacing, and when decreasing the fin height. Compared to the upward conditions, the downward trend is shifted down. As even previously pointed out, each trend of heat transfer coefficient reaches a maximum at high temperature, before decreasing. The down-shifting is similar to that occurring for heated horizontal plates [26]. When the heated surface faces downwards, the plate itself represents an obstacle to the tendency of the warm air to ascend, lowering the heat transfer. In upwards configuration, instead, the heat transfer is due to descending and ascending columns of cold and warm fluids respectively: because of the space vacated by the heated fluid is occupied by the cooler, heavier fluids, the heat transfer is more effective.

4.5. Combined convective and radiative heat transfer

In 2010, Khor et al. [27] highlighted that the effects of thermal radiation have been often neglected when the natural convection has been studied. The authors found out that ignoring the contribution of the radiative heat transfer can lead to errors higher than 30% in calculating the heat transfer coefficients. On the other hand, considering the radiation without adequately view factors can instead increase the error up to 60%. For this reason, in this work, the contribution of radiative heat transfer has been accurately estimated using referenced methods [10,19] and then used to calculate the amount of heat transferred by convection.

The present study has been primarily focused on the study of convective heat transfer and on the development of a new correlation to determine the Nusselt number at micro-scale. Therefore, the study presented so far has been conducted on the portion of heat that micro-fins transfer by convection only. So, the radiative heat transfer, calculated as for (4), has been used in (2) to determine the convective heat transfer. In order to give a more accurate description of the heat transfer taking place a micro-scale, the contribution of radiative heat transfer of a micro-finned heat sink under natural convection conditions is studied in this section. The results of the present experimental investigation confirm the important contribution of the radiative exchange in a micro-heat sink in natural convection conditions, in accordance with the numerical investigation presented in [15]. In that study, the authors modeled a 10 mm width and 40 μm heat sink with an emissivity of 0.70 and predicted a maximum radiative contribution of 22% for power inputs between 1.7 and 1.8 mW and temperatures of 100 °C. In the conditions considered in the present work, instead, the radiative exchange contributes dissipating up to 56% of the heat, losses excluded, so it cannot be neglected when designing a micro-passive cooling system under natural convection. Fig. 17 show the combined convective and radiative heat transferred by the fins (Q_{tot}), as calculated in Eq. (22). The overall heat is compared with the contributions given by the radiative and the convective components. As expected, at high temperatures radiation contributes more than convection to heat transfer. The intersection point between the two trends varies at different geometries: when dimensioning a micro-finned heat sink, the contribution of the radiative exchange needs to be considered using one of the models available in literature.

The results of this investigation support the conclusions of [27] and extend them to micro-scaled heat transfer: radiation should not be neglected when the thermal behaviors of natural convective micro-finned heat sinks are studied. In this light, further works to improve the design of fins and micro-fins in order to optimize the combined contribution of convection and radiation are strongly recommended.

5. Conclusions

The introduction of micro-fins for passive cooling is a solution that might interest a wide range of applications, such as power electronics, LED and concentrating photovoltaics. The present work investigates the thermal behavior of micro-finned heat sink under natural convection conditions. The effects of fin geometry, orientation and materials are reported and discussed. In agreement with previous researches, the heat transfer coefficient has been found to increase when the spacing is increased and the fin height is decreased. Moreover, it has been shown that the same coefficient is enhanced by the thickness of the fins. In this light, a modified Nusselt correlation has been proposed and validated using data from the present and previous. The trend of the heat transfer coefficient at high temperature differences has been analyzed as well. The heat transfer coefficient increases up to maximum value, and then decreases. As expected, the orientation of the fin arrays plays a major role in the heat exchange: micro-finned arrays facing down show lower thermal performances. The percentage difference of the heat transfer coefficients between upward and downward facing fins has been found to be consistent for each geometry at different power loads. To conclude, the radiative heat transfer can contribute up to the 60% of the net thermal exchange, and, thus, cannot be neglected when designing a micro-finned heat sink. More investigations on fin geometries, temperature ranges and materials need to be conducted, in order to find out the optimum design for a micro-finned heat sink in natural convection. Furthermore, taking into account also different heating conditions, such as a non-uniform heat sources, would lead to novel essential results to widen the knowledge of natural convective micro-fins.

Conflict of interest

None declared.

Acknowledgments

The financial support provided by the EPSRC-DST through the BioCPV project (Ref No: EP/J000345/1) is duly acknowledged. The authors wish to remark the importance of Mr. Ian Faulks' technical support. Leonardo Micheli would like also to thank Sam Lanyon from Concept Shed (UK) for the precious advices.

References

[1] N. Nagarani, K. Mayilsamy, A. Murugesan, G.S. Kumar, Review of utilization of extended surfaces in heat transfer problems, Renew. Sustain. Energy Rev. 29 (2014) 604–613, http://dx.doi.org/10.1016/j.rser.2013.08.068.

[2] A. Bar-Cohen, M. Iyengar, A.D. Kraus, Design of optimum plate-fin natural convective heat sinks, J. Electron. Packag. 125 (2003) 208, http://dx.doi.org/10.1115/1.1568361.

[3] A. Bar-Cohen, M. Iyengar, Design and optimization of air-cooled heat sinks for sustainable development, IEEE Trans. Compon. Packag. Technol. 25 (2002) 584–591, http://dx.doi.org/10.1109/TCAPT.2003.809112.

[4] A. Dayan, R. Kushnir, G. Mittelman, A. Ullmann, Laminar free convection underneath a downward facing hot fin array, Int. J. Heat Mass Transf. 47 (2004) 2849–2860, http://dx.doi.org/10.1016/j.ijheatmasstransfer.2004.01.003.

[5] K.H. Do, T.H. Kim, Y.-S. Han, B.-I. Choi, M.-B. Kim, General correlation of a natural convective heat sink with plate-fins for high concentrating photovoltaic module cooling, Sol. Energy 86 (2012) 2725–2734, http://dx.doi.org/10.1016/j.solener.2012.06.010.

[6] I. Tari, M. Mehrtash, Natural convection heat transfer from horizontal and slightly inclined plate-fin heat sinks, Appl. Therm. Eng. 61 (2013) 728–736, http://dx.doi.org/10.1016/j.applthermaleng.2013.09.003.

[7] I. Tari, M. Mehrtash, Natural convection heat transfer from inclined plate-fin heat sinks, Int. J. Heat Mass Transf. 56 (2013) 574–593, http://dx.doi.org/10.1016/j.ijheatmasstransfer.2012.08.050.

[8] J. Yeom, M.A. Shannon, 3.16 Micro-Coolers, in: Y. Gianchandani, O. Tabata, H. Zappe (Eds.), Compr. Microsystems, Elsevier, New York, 2007, pp. 499–550.

[9] L. Rick Wang, Y. Jaluria, Advances in Micro/Nanoscale Heat and Mass Transfer, J. Heat Transfer 137 (2015) 90301.

[10] D.P. Kulkarni, D.K. Das, Analytical and numerical studies on microscale heat sinks for electronic applications, Appl. Therm. Eng. 25 (2005) 2432–2449, http://dx.doi.org/10.1016/j.applthermaleng.2004.12.010.

[11] L. Micheli, S. Senthilarasu, K.S. Reddy, T.K. Mallick, Applicability of silicon micro-finned heat sinks for 500× concentrating photovoltaics systems, J. Mater. Sci. 50 (2015) 5378–5388, http://dx.doi.org/10.1007/s10853-015-9065-2.

[12] H. Ye, G. Zhang, A review of passive thermal management of LED module, J. Semicond. 32 (2011) 014008, http://dx.doi.org/10.1088/1674-4926/32/1/014008.

[13] A. Royne, C.J. Dey, D.R. Mills, Cooling of photovoltaic cells under concentrated illumination: a critical review, Sol. Energy Mater. Sol. Cells 86 (2005) 451–483, http://dx.doi.org/10.1016/j.solmat.2004.09.003.

[14] L. Micheli, N. Sarmah, X. Luo, K.S. Reddy, T.K. Mallick, Opportunities and challenges in micro- and nano-technologies for concentrating photovoltaic cooling: a review, Renew. Sustain. Energy Rev. 20 (2013) 595–610, http://dx.doi.org/10.1016/j.rser.2012.11.051.

[15] H. Shokouhmand, A. Ahmadpour, Heat Transfer from a micro fin array heat sink by natural convection and radiation under slip flow regime, Proc. World Congr. Eng. (2010).

[16] J.S. Kim, B.K. Park, J.S. Lee, Natural convection heat transfer around microfin arrays, Exp. Heat Transf. 21 (2008) 55–72, http://dx.doi.org/10.1080/08916150701647835.

[17] S. Mahmoud, R. Al-Dadah, D.K. Aspinwall, S.L. Soo, H. Hemida, Effect of micro fin geometry on natural convection heat transfer of horizontal microstructures, Appl. Therm. Eng. 31 (2011) 627–633, http://dx.doi.org/10.1016/j.applthermaleng.2010.09.017.

[18] N.M. Ravindra, B. Sopori, O.H. Gokce, S.X. Cheng, A. Shenoy, L. Jin, et al., Emissivity measurements and modeling of silicon-related materials : an overview 1 (22) (2001) 1593–1611.

[19] N.V. Suryanarayana, Engineering Heat Transfer, West Publishing Company, 1995.

[20] T. Fujii, H. Imura, Natural-convection heat transfer from a plate with arbitrary inclination, Int. J. Heat Mass Transf. 15 (1972) 755–767.

[21] T.A. Reddy, Applied Data Analysis and Modeling for Energy Engineers and Scientists, Springer Science & Business Media, 2011.

[22] J.P. Holman, Heat Transfer, Tenth ed., McGraw-Hill, 2010.

[23] Y.A. Çengel, Introduction to Thermodynamics and Heat Transfer, second ed., McGraw-Hill, 2008.

[24] C.D. Jones, L.F. Smith, Optimum arrangement of rectangular fins on horizontal surfaces for free-convection heat transfer, J. Heat Transfer. 92 (1970) 6, http://dx.doi.org/10.1115/1.3449648.

[25] B. Govinda Rao, V. Dharma Rao, S.V. Naidu, K.V. Sharma, B. Sreenivasulu, Heat transfer from a vertical fin array by laminar natural convection and radiation-A quasi-3D approach, Heat Transf. Res. 40 (2011) 524–549, http://dx.doi.org/10.1002/htj.20360.

[26] F.P. Incropera, D.P. DeWitt, T.L. Bergman, A.S. Lavine, Fundamentals of Heat and Mass Transfer, Wiley, 2007.

[27] Y.K. Khor, Y.M. Hung, B.K. Lim, On the role of radiation view factor in thermal performance of straight-fin heat sinks, Int. Commun. Heat Mass Transf. 37 (2010) 1087–1095, http://dx.doi.org/10.1016/j.icheatmasstransfer.2010.06.012.